

RESEARCH ARTICLE

Understanding coastal wetland hydrology with a new regional-scale, process-based hydrological model

Yu Zhang¹  | Wenhong Li¹ | Ge Sun² | Guofang Miao³ | Asko Noormets⁴ | Ryan Emanuel³ | John S. King³

¹Earth and Ocean Sciences, Nicholas School of the Environment, Duke University, Durham, North Carolina

²Eastern Forest Environmental Threat Assessment Center, Southern Research Station, United States Department of Agriculture Forest Service, Raleigh, North Carolina

³Department of Forestry and Environmental Resources, North Carolina State University, Raleigh, North Carolina

⁴Department of Ecosystem Science and Management, Texas A&M University, College Station, Texas

Correspondence

Wenhong Li, Earth and Ocean Sciences, Nicholas School of the Environment, Duke University, Durham, NC 27708.
Email: wenhong.li@duke.edu

Funding information

Division of Earth Sciences, Grant/Award Number: EAR-1462169; Division of Emerging Frontiers, Grant/Award Number: EF-1427188; Lawrence Berkeley National Laboratory, Grant/Award Number: 2014-0500/7090112; National Institute of Food and Agriculture, Grant/Award Number: 2014-67003-22068

Abstract

Coastal wetlands represent an ecotone between ocean and terrestrial ecosystems, providing important services, including flood mitigation, fresh water supply, erosion control, carbon sequestration, and wildlife habitat. The environmental setting of a wetland and the hydrological connectivity between a wetland and adjacent terrestrial and aquatic systems together determine wetland hydrology. Yet little is known about regional-scale hydrological interactions among uplands, coastal wetlands, and coastal processes, such as tides, sea level rise, and saltwater intrusion, which together control the dynamics of wetland hydrology. This study presents a new regional-scale, physically based, distributed wetland hydrological model, PIHM-Wetland, which integrates the surface and subsurface hydrology with coastal processes and accounts for the influence of wetland inundation on energy budgets and evapotranspiration (ET). The model was validated using in situ hydro-meteorological measurements and Moderate Resolution Imaging Spectroradiometer (MODIS) ET data for a forested and herbaceous wetland in North Carolina, USA, which confirmed that the model accurately represents the major wetland hydrological behaviours. Modelling results indicate that topographic gradient is a primary control of groundwater flow direction in adjacent uplands. However, seasonal climate patterns become the dominant control of groundwater flow at lower coastal plain and land–ocean interface. We found that coastal processes largely influence groundwater table (GWT) dynamics in the coastal zone, 300 to 800 m from the coastline in our study area. Among all the coastal processes, tides are the dominant control on GWT variation. Because of inundation, forested and herbaceous wetlands absorb an additional 6% and 10%, respectively, of shortwave radiation annually, resulting in a significant increase in ET. Inundation alters ET partitioning through canopy evaporation, transpiration, and soil evaporation, the effect of which is stronger in cool seasons than in warm seasons. The PIHM-Wetland model provides a new tool that improves the understanding of wetland hydrological processes on a regional scale. Insights from this modelling study provide benchmarks for future research on the effects of sea level rise and climate change on coastal wetland functions and services.

KEYWORDS

coastal processes, coastal wetlands, flooding and inundation, hydrologic model, surface–subsurface interaction, wetland hydrology

1 | INTRODUCTION

Coastal wetlands represent some of the most productive ecosystems on Earth and provide important ecological services such as flood attenuation, water and carbon storage, shoreline stabilization, and wildlife habitat (Roulet, 1990; Tiner, 2013). For example, more than 50% of the commercially harvested fish in the United States live in coastal waters at some stage in their life cycles (NOAA Habitat Conservation, 2017). Coastal wetlands also act as a natural filter that improves water quality before it reaches the ocean (Kolb, 1974). Nearly two thirds of the human population lives and works within 150 km of a coastline (Hinrichsen, 1999), placing substantial pressure on coastal wetlands. Moreover, wetland ecological services are increasingly influenced by global environmental disturbances, including land use change (Kirwan & Megonigal, 2013; Pendleton et al., 2012), sea level rise (SLR; Cahoon et al., 2006; Moorhead & Brinson, 1995; Morris, Sundareshwar, Nietch, Kjerfve, & Cahoon, 2002), and intensified climate extremes and weather events (Dai et al., 2010; Day et al., 2008; Erwin, 2009).

Hydrological processes are the major driver of coastal wetlands function, affecting wetland formation, structure, productivity, and ecosystem services provisioning (Merken, Deboelpaep, Teunen, Saura, & Koedam, 2015; National Research Council, 1995; Tiner, 1999). Thus, understanding the mechanisms and dynamics of coastal wetland hydrology is a prerequisite to predicting how coastal wetlands will respond to natural and human-induced disturbances and, therefore, is vital for coastal wetland management.

On regional scales, ranging from tens of kilometres (Smith & Chapman, 1983) to thousands of kilometres (O'Neill et al., 1996), coastal wetlands are unique landscape components that link terrestrial ecosystems to the ocean. Hydrological variations of coastal wetlands (Figure 1) are strongly influenced by (a) coastal processes (i.e., tide, SLR, and saltwater intrusion (Yu et al., 2016)), (b) near-shore climate (Woo, 1992), and (c) hydrological processes from adjacent upland terrestrial ecosystems (Ataie-Ashtiani, Volker, & Lockington, 1999). Notably, land cover properties of coastal wetlands may vary due to

inundation (see Figure 1 inset), which can influence wetland energy budgets by altering surface albedo, emissivity, and heat capacity (Sumner, Wu, & Pathak, 2011). In addition, wetland evaporation and transpiration may change due to the submergence of roots and even whole plant canopies. However, changes in energy budgets and evapotranspiration (ET) partitioning in response to inundation of coastal wetlands have not been systematically investigated, especially at the regional scale.

To date, many hydrological models have been developed to describe coastal wetland hydrology (Dai et al., 2010; La Torre Torres, Amatya, Sun, & Callahan, 2011; Li, Barry, & Pattiaratchi, 1997; Li, Barry, Stagnitti, & Parlange, 1999; Lu, Sun, McNulty, & Amatya, 2003; Robinson, Gibbes, & Li, 2006; Sun, Riekerk, & Comerford, 1998; Yu et al., 2016; Yuan, Xin, Kong, Li, & Lockington, 2011; Zhu et al., 2017). Some of these models have physically based representations of hydrological processes (Dai et al., 2010; Li et al., 1997; Li et al., 1999; Robinson et al., 2006; Sun et al., 1998; Yu et al., 2015; Yuan et al., 2011). For example, Richards's equation and Darcy's law have been used for modelling subsurface and surface water flow (La Torre Torres et al., 2011; Yu et al., 2016). Alternatively, statistical models have been used to simulate and predict hydrological variables (e.g., groundwater table [GWT] depth) using empirical relationships between meteorological variables and hydrological states from site-specific measurements (La Torre Torres et al., 2011; Lu et al., 2003; Zhu et al., 2017). These wetland hydrological models were often developed for specific types of wetland ecosystems. For example, coastal marshes have been intensively studied using small-scale models (e.g., spatial scale of tens to hundreds of metres from the shoreline) to understand the variation of surface and subsurface flow under the microtopographic control, and how water flow influences the distribution and transport of salt water and nutrients (Li et al., 1997; Li et al., 1999; Oude Essink, Van Baaren, & De Louw, 2010; Yu et al., 2015; Yu et al., 2016; Yuan et al., 2011). Watershed-scale models (e.g., spatial scale of thousands of square metres) have been employed to understand variation in ET and the GWT of forested wetlands under climate variability/change (Dai et al., 2010; La Torre Torres et al., 2011; Lu et al., 2003; Sun et al., 1998; Zhu et al., 2017).

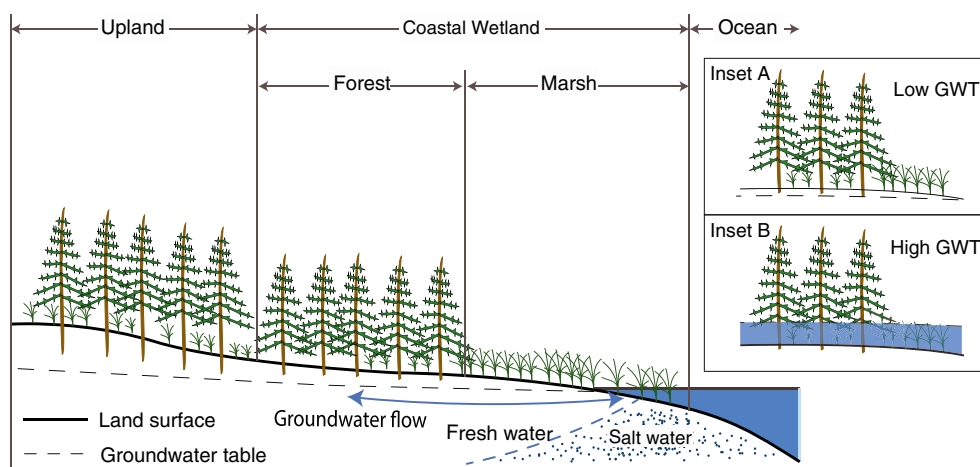


FIGURE 1 Illustration of the surface and subsurface hydrological processes for a coastal wetland system. Inset figures A and B illustrate the coastal wetland under the low and high water levels, respectively

However, coastal marshes and forested wetlands are not hydrologically isolated. Previous models have been unable to adequately describe full coastal wetland hydrological processes and interactions among upland terrestrial landscapes, coastal-forested wetlands, coastal herbaceous wetlands, and the ocean at the regional scale (Figure 1). Investigating wetland function/hydrological processes at the regional scale is key to systematically understanding how coastal wetlands respond to broad-scale environmental change and SLR.

The objective of this study is to develop a physically based, regional-scale model (PIHM-Wetland) that (a) couples coastal processes with surface and subsurface hydrological dynamics and simulates water exchange among coastal marshlands, coastal-forested wetlands, upland terrestrial landscapes, and the ocean; (b) tracks changes to wetland energy budgets and ET partitioning caused by inundation; and (c) provides better understanding of the spatial and temporal dynamics of coastal wetland hydrology by answering the following questions:

- Will modelling of regional-scale hydrological interactions significantly improve understanding of the hydrodynamics of coastal wetlands relative to currently available models?
- How do coastal processes (tides, SLR/inundation, saltwater intrusion) affect wetland energy budgets, ET, and surface/subsurface hydrodynamics?
- How do proximity to the shoreline, spatial domain (e.g., area), and adjacent ecosystems affect wetland GWT dynamics?

2 | MODEL DEVELOPMENT

Based on the major components of the surface and subsurface hydrological processes in the Penn State Integrated Hydrological Model (PIHM; Qu & Duffy, 2007), this study developed a wetland hydrology model (named PIHM-Wetland) representing a regional-scale, spatially distributed, and physically based model. PIHM-Wetland tracks the change in water storage from the vegetation canopy, ground surface, unsaturated soil zone, and saturated soil zone by using the semidiscrete finite volume method and triangular irregular network (TIN). The reasons for adopting PIHM to develop PIHM-Wetland include the following: (a) PIHM has a detailed representation of the surface and subsurface hydrological processes (Li et al., 2017; Shi et al., 2015; Yu, Duffy, Baldwin, & Lin, 2014; Yu, Duffy, Zhang, Bhatt, & Shi, 2016; Zhang, Slingerland, & Duffy, 2016); (b) TIN is flexible for delineating complex terrain, such as irregular boundaries, water bodies, and heterogeneous land surface properties (Kumar, Bhatt, & Duffy, 2009) and extending to large spatial scales (Braun & Sambridge, 1997; Zhang et al., 2016); (c) PIHM is a community-based model with implementations and module extensions across disciplines (Bao, Li, Shi, & Duffy, 2017; Li & Duffy, 2011; Liu & Kumar, 2016; Shi, Davis, Duffy, & Yu, 2013; Yu et al., 2014; Zhang et al., 2016); and (d) PIHM is well supported by a set of preprocess tools (e.g., PIHM-GIS, Kumar et al., 2009; and the HydroTerre national dataset platform, <http://www.hydroterre.psu.edu>; Leonard & Duffy, 2013).

In its original form, PIHM focuses on hydrological simulation of a single watershed with relatively simple boundary settings (e.g., zero-

flow boundary condition at watershed boundary). In our modification, PIHM-Wetland is designed as a regional-scale model that takes into account surface and subsurface water exchange between watersheds. Additionally, PIHM-Wetland fully couples the coastal processes of tides, SLR, and saltwater intrusion and considers the effects of inundation on coastal wetland hydrology, which were not considered in PIHM.

2.1 | Hydrological components

PIHM-Wetland simulates the hydrological cycle including canopy interception, snowmelt, infiltration, recharge, ET, overland flow, surface water routing, and lateral groundwater flow by integrating the underlying ordinary and partial differential equations (ODEs and PDEs, respectively) in a fully coupled scheme (Qu & Duffy, 2007). In addition to these coupled processes in the original PIHM, the process of saltwater intrusion is newly integrated. Based on the conservation of mass of water, the generic form of the governing equations for PIHM-Wetland is

$$\left\{ \begin{array}{l} \frac{dS_{\text{canopy}}}{dt} = vFrac * (1 - sFrac) * P - E_c \\ \frac{dS_{\text{snow}}}{dt} = sFrac * P - SM \\ \frac{\partial S_{\text{surf}}}{\partial t} = TF - \nabla q_{\text{sw}} - I - E_s \\ \frac{dS_{\text{unsat}}}{dt} = I - R - E_g - E_{\text{gt}} \\ \frac{\partial S_{\text{sat}}}{\partial t} = -\nabla q_{\text{gw}} + R - E_{\text{sat}} - E_{\text{tsat}} \\ \frac{\partial S_{\text{salt}}}{\partial t} = -\nabla q_{\text{salt}} \end{array} \right. \quad (1)$$

where $\frac{dS_{\text{canopy}}}{dt}$ represents the time rate of change of the canopy water storage, S_{canopy} (m), due to canopy evaporation E_c (m/day) and canopy interception $vFrac * (1 - sFrac) * P$ (m/day). $vFrac$ and $sFrac$ are the vegetation fraction and snow fraction, respectively. P is precipitation (m/day). $\frac{dS_{\text{snow}}}{dt}$ describes the time rate of change of snow storage S_{snow} (m) due to $sFrac * P$, snow formation from precipitation when temperature is below 0°C (m/day), and SM , snow melt (m/day), which is a function of degree-day factor of ice and snow melt (Kumar, 2009). $\frac{\partial S_{\text{surf}}}{\partial t}$ represents the time rate of change of surface water storage, S_{surf} (m), due to TF , throughfall (m/day); ∇q_{sw} , net overland flow (m/day); I , infiltration (m/day); and E_s , surface water evaporation (m/day). ∇q_{sw} is modelled by the diffusion wave approximation of St. Venant's equation assuming shallow surface water depth and negligible influence of inertia force on overland flow, which is equivalent to Manning's equation (Zhang et al., 2016). The estimation of infiltration rate is a function of the gradient of the surface and subsurface hydraulic head. $\frac{dS_{\text{unsat}}}{dt}$ represents the time rate of change of unsaturated water storage (m) due to I , infiltration (m/day); R , recharge (m/day); E_g , soil evaporation (m/day); and E_{gt} , transpiration (m/day). The recharge is calculated using Richard's equation assuming a vertical exchange of water across a moving water table interface (Kumar, 2009). At last, $\frac{\partial S_{\text{sat}}}{\partial t}$ and $\frac{\partial S_{\text{salt}}}{\partial t}$ represent the time rate of change of the saturated water storage, S_{sat} (m), and the saltwater storage, S_{salt} (m), respectively.

∇q_{GW} is net groundwater lateral movement between adjacent cells (m/day) represented by the Darcy-type flow proportional to groundwater gradient. E_c , E_s , E_g , and E_{sat} are the evaporation (m/day) from the vegetation canopy, surface water, unsaturated soil zone, and saturated soil zone, respectively. The potential evaporation rate is estimated by the Penman equation (Zhang, Yang, Ouyang, Zeng, & Cai, 2010). The transpiration (m/day) is described by E_{gt} or E_{tsat} , depending upon the vegetation coverage, the rooting depth, and the GWT. If the GWT is higher than rooting depth, plants uptake water from the saturated zone, and E_{tsat} applies. Otherwise, water uptake occurs at the unsaturated soil zone, and E_{gt} applies. A detailed calculation of each parameter is provided in the Supporting Information and the literature (Kumar, 2009; Qu & Duffy, 2007; Van Genuchten, 1980; Zhang et al., 2010; Zhang et al., 2016).

2.2 | New wetland module

A new wetland module was designed and added into the hydrological components. The land cover properties of wetlands, especially for coastal wetlands, are likely to vary due to inundation (see the inset in Figure 1). PIHM-Wetland tracks the influences of inundation on wetland hydrology from two aspects: (a) the impact of inundation on canopy evaporation and transpiration and (b) the impact of inundation on net radiation.

The transpiration rate is determined by the vapour pressure gradient (VPG) between plant stomata and the atmosphere (Taiz, Zeiger, Møller, & Murphy, 2015). During inundation, with the decrease of VPG, the transpiration rate decreases dramatically and even drops to zero for submerged plants (Rawson, Begg, & Woodward, 1977). Thus, the phenomenon is expressed as

$$E_{\text{gt}} \text{ or } E_{\text{tsat}} = \begin{cases} v\text{Frac} \frac{\Delta[R_n - G] + \left(\frac{\rho_a C_p}{r_a}\right)(\epsilon_s - \epsilon_a)}{\Delta + \gamma\left(1 + \frac{r_s}{r_a}\right)} (1 - \delta_r) & \psi_{\text{surf}} < h_{\text{plant}} \\ 0 & \psi_{\text{surf}} \geq h_{\text{plant}} \end{cases} \quad (2)$$

where h_{plant} is the height of plant canopy (m). When surface water level (SWL) is lower than vegetation canopy height, the estimation of transpiration rate follows the Penman equation. However, the transpiration rate equals to zero when vegetation canopy is submerged in water. Likewise, the canopy evaporation drops to zero when surface water covers the whole canopy layer. In this study, the influence of inundation on soil evaporation is not discussed further because inundation that makes the soil evaporation equal to open-water evaporation has been well studied (Rebelo, Senay, & McCartney, 2012; Sánchez-Carrillo, Angeler, Sánchez-Andrés, Alvarez-Cobelas, & Garatuza-Payán, 2004; Schwerdtfeger, da Silveira, Zeilhofer, & Weiler, 2015) and is already considered in PIHM.

For the second aspect, inundation changes the reflectivity of the land surface (also called albedo) resulting in the change of the surface energy budget by absorbing and reflecting differing amounts of radiation (Sumner et al., 2011). PIHM-Wetland checks the surface water depth before calculating the net solar radiation at each time step. The albedo is set to be 0.06 for the land surface where the surface

water depth is greater than the default depth (Li & Garand, 1994). Here, the default depth is 0.01 m, and it can vary for different landscapes. The equation yields

$$\alpha_{\text{new}} = \begin{cases} \alpha & 0 \leq S_{\text{surf}} < 0.01 \\ \alpha * v\text{Frac} + 0.06 * (1 - v\text{Frac}) & 0.01 \leq S_{\text{surf}} < h_{\text{plant}} \\ 0.06 & S_{\text{surf}} \geq h_{\text{plant}} \end{cases} \quad (3)$$

where α is the original albedo of land surface. α_{new} is the new albedo. Note that the canopy height does not have to be always higher than the default depth (0.01 m here). If h_{plant} is lower than the default surface water depth, the equation can be expressed as

$$\alpha_{\text{new}} = \begin{cases} \alpha & 0 \leq S_{\text{surf}} < h_{\text{plant}} \\ 0.06 & S_{\text{surf}} \geq h_{\text{plant}} \end{cases} \quad (4)$$

This study used a fixed value (0.9) for land surface emissivity because this parameter for different land cover types is very similar, around 0.9 (Li et al., 2013).

2.3 | Coastal flow boundary conditions

PIHM-Wetland integrates the coastal hydrological boundary conditions of tides and SLR into the model. The coastal boundary condition on a model domain $\Omega \subset \mathbb{R}^n$ takes the form

$$q_{\text{sw}}(x) = \frac{[S_{\text{surf}}(x)]^{\frac{5}{2}} (S_{\text{surf}}(x) + z - h_{\text{sea}}) / L}{n_s * (m)^{\frac{3}{2}}} \quad \forall x \in \partial\Omega, \quad (5)$$

where z is the land surface elevation (m), h_{sea} is the sea level (m) on the boundary $\partial\Omega$, L is the distance between the boundary element and the ocean, n_s is Manning's roughness, and m is the surface slope.

Additionally, the density difference between fresh water in the aquifer and salt water in ocean results in the pressure difference between fresh water and salt water, triggering the motion of salt water into the aquifer (Gupta, 1985). The fresh water and salt water form a dynamic freshwater-saltwater interface (the blue dashed line in Figure 1) assuming that (a) the fresh and salt water are immiscible by ignoring the dispersion between the interface and (b) the flow is Dupuit flow where the hydraulic head along a vertical direction is constant (Michael, Mulligan, & Harvey, 2005; Shamir & Dagan, 1971). Here, we take the form suggested by (Shamir & Dagan, 1971) to track the motion of the interface:

$$q_{\text{gw}}(x) = -K \frac{\partial(S_{\text{sat}}(x) + S_{\text{salt}}(x) + z_b)}{\partial x} \quad \forall x \in \partial\Omega, \quad (6)$$

$$q_{\text{salt}}(x) = -K \frac{\partial \left[\frac{\sigma_f S_{\text{sat}}(x)}{\sigma_s} + S_{\text{salt}}(x) \right]}{\partial x} \quad \forall x \in \partial\Omega, \quad (7)$$

where K is the hydraulic conductivity (m/day). σ_f and σ_s are the density of fresh and salt water (kg/m^3), respectively. In this study, $\sigma_f = 1,000 \text{ kg/m}^3$ and $\sigma_s = 1,025 \text{ kg/m}^3$.

2.4 | Domain decomposition and numerical method

PIHM-Wetland decomposes a model domain into unstructured TIN by using the Delaunay triangulation. The size of the triangles is

automatically controlled by the heterogeneity of the land cover and research interests, such as streams, open water, observation sites, and different land use types. The solutions are based on the decomposed domain using the finite volume method, where the original ODEs and PDEs are integrated over the control volume and converted to semidiscrete ODEs. The semidiscrete governing equations representing the hydrological processes for each control volume are then assembled to a global ODE system and solved simultaneously using the Newton–Krylov implicit ODE solver CVODE (Cohen & Hindmarsh, 1996). CVODE is a large-scale non-linear stiff ODE solver that combines the backward difference formula with linear Krylov iteration, and a preconditioned generalized minimal residual method algorithm (Byrne, 1992). The steps of discretizing the original governing equations are introduced in the literature (Kumar, 2009; Zhang et al., 2016).

3 | MODEL APPLICATION

We first evaluated the model performance using observational data from a coastal wetland in North Carolina, USA. The calibration and validation of the model were performed by comparing the simulated GWT, ET, soil water content (SWC), and SWL with in situ observations and remote sensing products.

3.1 | Site description

The study site is a coastal bottomland hardwood wetland and coastal marsh in the Alligator River National Wildlife Refuge (Figure 2a) on the Albemarle-Pamlico Peninsula in Dare County, North Carolina (see Figure 2a) with a total area of 2,784.4 km² and a maximum east–west distance of approximately 70 km. This research site is referred to as

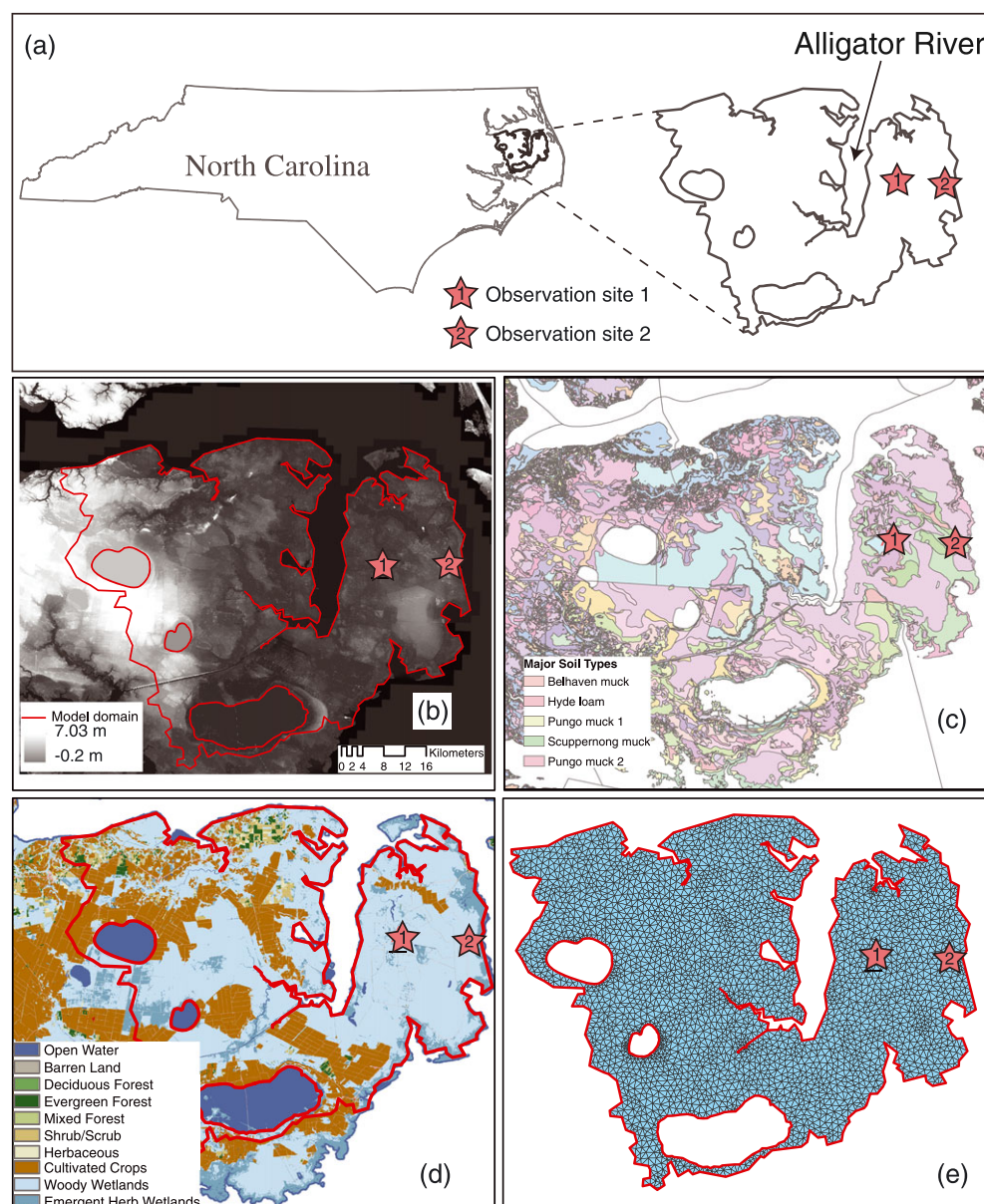


FIGURE 2 Study area (35°24′48″N, 76°40′15″W–36°5′11″N, 75°40′33″W). (a) The geographic location of the study area. (b) The topographic map with the model domain. (c) Soil types. (d) Land cover types. (e) Decomposed model domain with a triangular mesh. The red stars numbered “1” and “2” indicate the forested wetland observation site (35°46′34″N, 75°54′12″W), measuring energy and water fluxes and groundwater level, and the coastal herbaceous wetland site (35°46′5″N, 75°45′0″W), measuring water level, respectively

Alligator River Coastal Wetland (ARCW) in this study. The elevation relief of the model domain is about 7 m from the west upland to the east coast (Figure 2b). Based on its elevation distribution, the domain can be roughly classified as upland (light colour region in Figure 2b), forested wetland (dark grey colour in Figure 2b), and coastal herbaceous wetland near the land–ocean interface (darker blue colour in Figure 2d). The hydrological dynamics of ARCW is mainly driven by climate variabilities and coastal processes (Miao et al., 2013). To calibrate the model and validate the spatial representation of the model simulation across the model domain, this study used the observations from two available sites. The first observation site (marked as red star “1” in Figure 2) is a forested wetland where an eddy covariance flux tower was installed to measure energy fluxes, above-canopy humidity, CO₂ flux, above-canopy precipitation, and above-canopy air temperature. A ground weather station was also installed to measure near-ground precipitation, temperature, and humidity. Additionally, pressure transducers with data logger (several metres deep) and soil moisture sensors at the topsoil layer (0–0.3 m) were installed for the measurements of GWT and SWC, respectively. The second observation site (marked as red star “2” in Figure 2) is a coastal herbaceous wetland providing the measurement of SWL.

The mean annual air temperature is 16.9°C (from 1971 to 2000) with 6.8°C in January and 26.5°C in July (Miao et al., 2013). The mean annual precipitation is 1,270 mm with storms and hurricanes in the summer seasons (Li, Li, Fu, Deng, & Wang, 2011; Miao et al., 2013). The GWT varied between –0.3 m for the summer season and 0.3 m for the winter season (positive and negative signs mean GWT above and below ground surface, respectively) during the period of 2009–2011. The tree density around Observation Site 1 is 2,320 ± 800 stems/ha (Miao et al., 2013). Soils at this area are rich in organic matter with high porosity and permeability, especially for the top layer (0.2–0.3 m below ground surface; Miao et al., 2013).

3.2 | National database

To conduct the numerical experiment for the study area, several national datasets were used to represent soil properties, land cover characteristics, vegetation height, topography, tide, and meteorological forcing.

3.2.1 | Land surface properties

Soil properties

The soil parameters of PIHM-Wetland include soil texture, saturated water content, residual water content, air-entry suction, and pore size distribution. The numerical experiments in this study used the gSSURGO national soil database as the source of soil data (Staff, 2016). The ARCW is mainly covered by muck (hydric soil) with rich organic matter content at the surface (Moorhead & Brinson, 1995; Figure 2c and Table S1). The topsoil layer (0–0.3 m) is well drained because of coarse organic matter content, whereas the bottom layer (0.3–1 m) is poorly drained substrate, consistent with the studies by Bruland and Richardson (2006) and Moorhead and Brinson (1995) for coastal wetlands of North Carolina. The vertical and horizontal hydraulic conductivity and the van Genuchten water retention

parameters, α and n , respectively (listed in Table S1), were estimated by using the empirical pedotransfer function, a function of soil texture, organic matter content, and bulk density (Wösten, Pachepsky, & Rawls, 2001).

Land cover properties

The land cover parameters include maximum leaf area index, minimum stomatal resistance, reference stomatal resistance (Dickinson, Henderson-Sellers, & Kennedy, 1993; Sellers, Mintz, Sud, & Dalcher, 1986), albedo, vegetation fraction, Manning's roughness, and root zone depth. Here, we used the 2011 National Land Cover Database (NLCD) as the source of land cover data (Fry et al., 2011). There are 10 land cover types in the study area, including open water, barren land, deciduous forest, evergreen forest, mixed forest, shrub/scrub, herbaceous, cultivated crops, woody wetlands, and emergent herb wetlands (see Figure 2d and Table S2). Forested and herbaceous wetlands cover 75% and 3% of the study area, respectively. The temporal variation of these land cover parameters was derived from the NLCD land cover data and the Mapped Monthly Vegetation Data of different land cover types from National Aeronautics and Space Administration (Land Data Assimilation System, 1999), which are widely used in the parameterization of land surface models (Chen et al., 1996; Koster & Suarez, 1992; Niu et al., 2011).

Vegetation height

To evaluate the influence of flooding and inundation on different land covers with different canopy height, PIHM-Wetland introduced vegetation height as a parameter in the calculation of ET, which was not included in the original PIHM model. The LANDFIRE (LF) program provides high-resolution (30-m) geospatial layers, databases, and models for the entire United States (Rollins, 2009). The existing vegetation height (EVH) data is one of the essential parameters in the LF program providing the canopy height of vegetation. As the land cover type of EVH is well aligned with NLCD, this study used EVH as the vegetation height data for our study. According to EVH and NLCD, the vegetation type transits from reed and grass near the coastline (canopy height of 0.1 to 0.6 m) to tupelo, maple, cypress, and pine at the upland area (canopy height of 15 to 20 m).

3.2.2 | Climate and sea level databases

Meteorological forcing

The meteorological input data for PIHM-Wetland simulation are precipitation, surface air temperature, relative humidity, wind speed, incoming shortwave (SW) radiation, and incoming longwave radiation. The numerical experiments here used the North American Land Data Assimilation System Phase 2 (NLDAS-2) dataset from 2007 to 2016 with a spatial resolution of 0.125 degree and temporal resolution of 1 hr as meteorological forcing. Based on the availability of observation data, the accuracy of three meteorological forcing variables was evaluated by comparing it with the field measurements in Observation Site 1 from 2009 to 2011 (see Figure 3). Figure 3 indicates that both simulated temperature and relative humidity agree with the observations. There is a relatively large divergence in the daily precipitation comparison (Figure 3a), but good agreement in the weekly

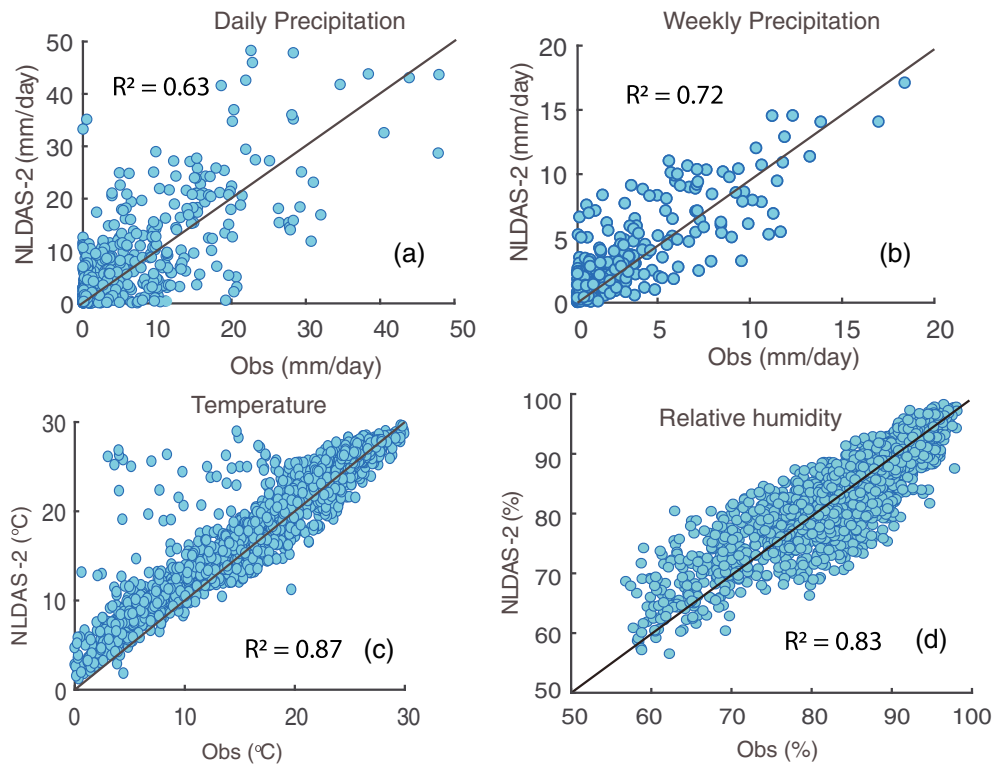


FIGURE 3 Comparison of the forcing data between NLDAS-2 product and observation from 2009 to 2011 at Observation Site 1 (35°47'N, 75°54'W). (a) Daily precipitation (mm/day), (b) weekly precipitation (mm/day), (c) daily temperature (°C), and (d) daily relative humidity. NLDAS-2: North American Land Data Assimilation System Phase 2

precipitation comparison (Figure 3c). As the four-way radiation sensor was not installed during the period of the numerical experiment, we were not able to compare the incoming and outgoing SW and longwave radiation separately.

Coastal tide and SLR

This study compiled the mean sea level trend (MSLT) and tide input data from the closest NOAA observation station (15 km from the boundary; Oregon Inlet Marina station of North Carolina, Station ID: 8652587; <https://tidesandcurrents.noaa.gov/>). The MSLT (unit: m) follows a linear function, $MSLT = \frac{0.0003t}{43,200} + 0.05971$, where t (min) is the time from 2007 to 2016 ($t = 0$ on January 1, 2007).

3.3 | Model set-up

The model domain was decomposed into 6,290 unstructured irregular triangular elements with a closed boundary condition, except a Dirichlet boundary condition (open boundary) for the elements along the coastline (Figure 2e). The averaged cell size is about 100 m determined by the acceptable computational time and the heterogeneity of the land cover and soil. The soil becomes poorly drained at about 1-m depth from the ground surface, below which the soil has little influence on the overall hydrological behaviour of the system. Thus, the numerical experiments focused on the hydrological processes within the top 1-m soil layer. The initial GWT was set as 0.1 m below ground surface and no initial surface water for the entire modelling domain. We set a constant lake level for the three lakes at the west side of the model domain. The open boundary is linked to sea level variation.

The initial saltwater depth was set to zero. At the boundary, the saltwater depth varies with the freshwater discharge following the rule

$$\psi_{\text{salt}}(0, t) = \frac{q_{\text{gw}}(0, t)}{K \frac{\sigma_s - \sigma_f}{\sigma_f}}, \quad (8)$$

where $\psi_{\text{salt}}(0, t)$ is the saltwater depth (m) at the land-ocean boundary, q_{gw} is the groundwater flux at the boundary (m^2/day), K is hydraulic conductivity (m/day), and σ_f and σ_s are density of fresh water and salt water (kg/m^3), respectively. The simulation time interval was 1 min, and the output time interval was 1 day. We first ran the model towards an equilibrium state and then started the real simulation by using the meteorological forcing from 2007 to 2016.

3.4 | Model calibration and validation

PIHM-Wetland was calibrated and validated by comparing the simulated ET and GWT with in situ measurements at the observation sites as well as with satellite products for the entire region. We manually tuned the seven key model parameters, including horizontal and vertical soil hydraulic conductivity, hydraulic conductivity for infiltration, porosity, air-entry suction, pore size distribution, and Manning's roughness, by using the observed ET, GWT, and SWC of 2009 at Observation Site 1 and the observed SWL of 2015 at Observation Site 2. Streamflow observations were not available in the study area for calibration and validation. The upper and lower bounds of the seven key parameters were well quantified in the earlier model applications (Shi et al., 2015; Yu et al., 2016; Yu, Duffy, Baldwin, & Lin, 2014). The parameters were tuned manually on the basis of

the objective function of Nash–Sutcliffe efficiency (NSE; Nash & Sutcliffe, 1970).

$$NSE = 1 - \frac{\sum (Obs - Sim)^2}{\sum (Obs - Mean_{obs})^2}, \quad (9)$$

where an NSE of 1 corresponds to a perfect match of model simulation to observation. In general, a model simulation is considered as a

reasonable simulation when NSE is above 0.5 (Moriya et al., 2007; Vergnes et al., 2012).

The model simulation was validated by using the observed ET, GWT, and SWC in 2010 and 2011 from Observation Site 1 and the observed SWL in 2016 at Observation Site 2 (Figure 4). At the observation sites, the NSE values are 0.81, 0.93, 0.96, and 0.79 for simulated ET, GWT, SWC, and SWL, respectively, suggesting

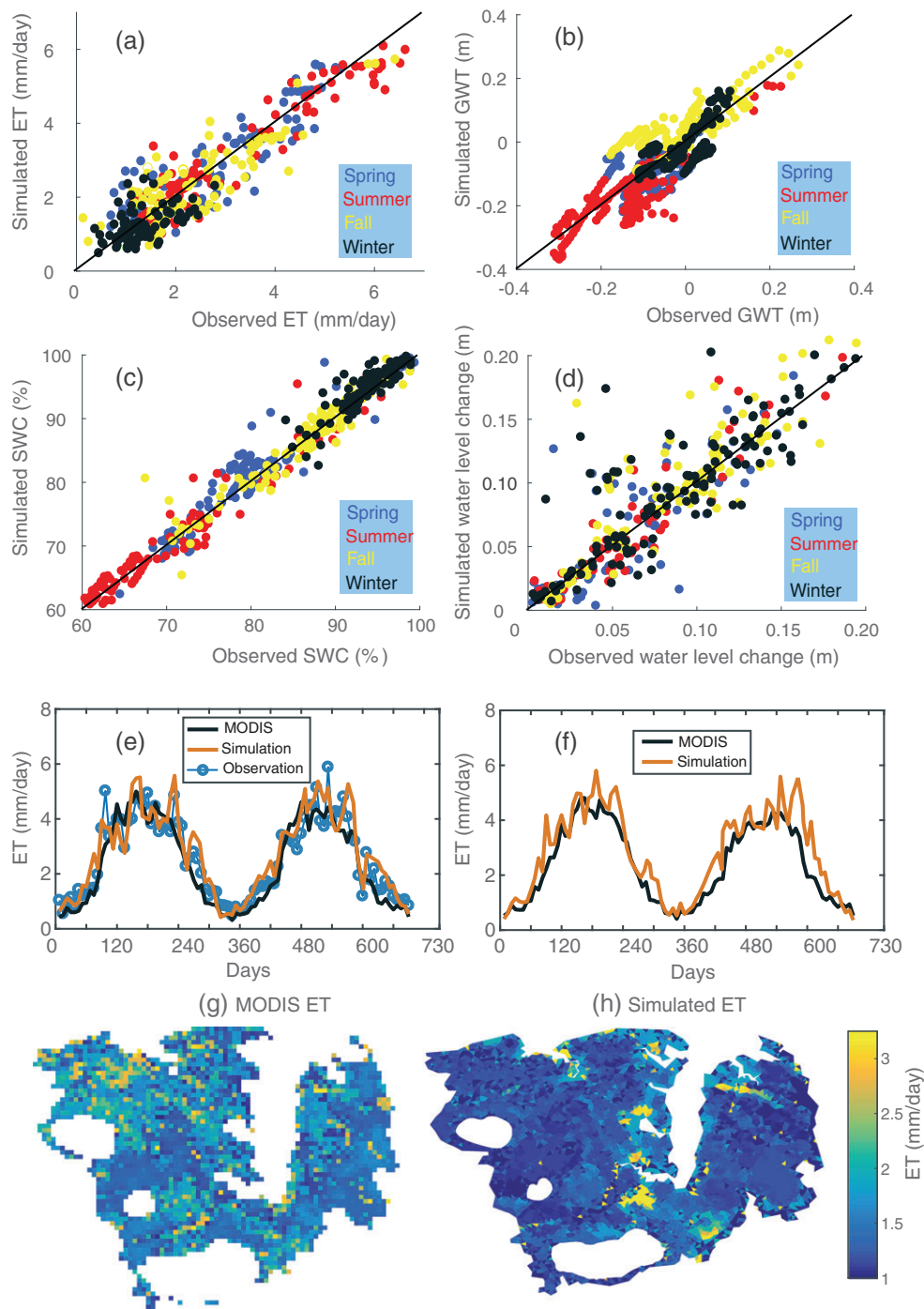


FIGURE 4 Model validation for ET, GWT, and SWC in 2010 and 2011 and for SWL in 2016. (a) Comparison of daily ET (mm/day) between simulation and in situ measurements at Observation Site 1 (see Figure 2a). (b) Same as (a) but for daily GWT (m). A positive value indicates that the GWT is above the ground surface. (c) Same as (a) but for daily SMC. (d) The comparison of daily SWL (m) between simulation and in situ measurements at Observation Site 2 (see Figure 2a). (e) Time series comparison of 8-day averaged ET among MOD16 product, simulation, and observation at the observation site. Day 0 (x-axis) refers to Jan 1, 2010. (f) The comparison of the domain-averaged 8-day ET between MOD16 and simulation. (g) Spatial distributed averaged ET of 2010 and 2011 from the MOD16 product. (h) Same as (g) but for the model simulation. ET: evapotranspiration; GWT: groundwater table; SWC: soil water content; SWL: surface water level

that the model is capable of providing reasonably accurate simulations of ET, GWT, SWC, and SWL. The relative SWL instead of the absolute water level was compared at Observation Site 2 because the datum for calculating the absolute water level was not available.

Simulated ET patterns were also compared with MOD16 ET products on regional scales (35°24'48"N, 76°40'15"W–36°5'11"N, 75°40'33"W). The MOD16 ET dataset is an 8-day averaged land surface ET product with a spatial resolution of 1 km (Mu, Zhao, & Running, 2011). Figure 4e shows that MOD16 ET agrees with the in situ measurement, though MOD16 ET did not capture some spikes in the time series of the observed ET. Figure 4f compares domain-averaged ET between the simulation and MOD16 ET product. They are well aligned, except for some peaks in the summer seasons presumably due to the differences of the meteorological forcing inputs and algorithm of calculating ET. Moreover, the comparison of the ET spatial distribution shows that the simulated and MOD16 ET products have similar magnitude and patterns: ET is higher near the coastal area (about 2.46 mm/day on average) and lower at the upland (approximately 1.51 mm/day, Figure 4g and h). Notably, MOD16 presented a higher ET at the northwest of the domain where farmland is located. The ET difference of the farmland is possibly attributed to the different ways of calculating ET between MOD16 and PIHM-Wetland, especially the difference in meteorological inputs and the calculation of SWC.

4 | RESULTS

After the model was tested, several numerical experiments were conducted to demonstrate the importance of the model improvements and to explore the characteristics of coastal wetland hydrology.

We first showed the simulated hydrodynamics of ARCW from 2007 to 2016 focusing on the regional-scale variation of groundwater flow (Section 4.1) and then estimated the impact area of coastal processes on GWT (Section 4.2). At last, we examined the influence of inundation on energy budget and ET partitioning (Section 4.3).

4.1 | Seasonal groundwater flow across a topographic gradient

The simulated groundwater flow vectors in the summer and winter seasons (Figure 5) were derived from the 10-year (2007–2016) averaged summer and winter GWT elevations. The analysis focused on summer and winter seasons because the groundwater flow in these two seasons sufficiently reflects distinct climate controls on groundwater dynamics. In both the summer (Figure 5a) and winter (Figure 5b) seasons, groundwater moves from the western upland (light blue and yellow in Figure 5) to the eastern coastal plain (dark blue in Figure 5) following the topographic gradient; the flow direction stays the same across the western upland area. However, in the eastern coastal plain where the topographic gradient is small, seasonal climate becomes the dominant control on groundwater flow. During summer months, the seasonal averaged GWT is about 0.1 m higher in the coastal herbaceous wetland than that in the forested wetlands. Salt water intrudes into the coastal herbaceous wetland from the ocean, and groundwater flows from the herbaceous wetland to the forested wetland to compensate the large water loss in summer (Figure 5a). In contrast, during winter, the groundwater flow becomes reversed in the coastal plain. The seasonal averaged GWT in the forested wetland is about 0.02 m higher than that in the coastal herbaceous wetland, such that the groundwater tends to move from the land to the ocean.

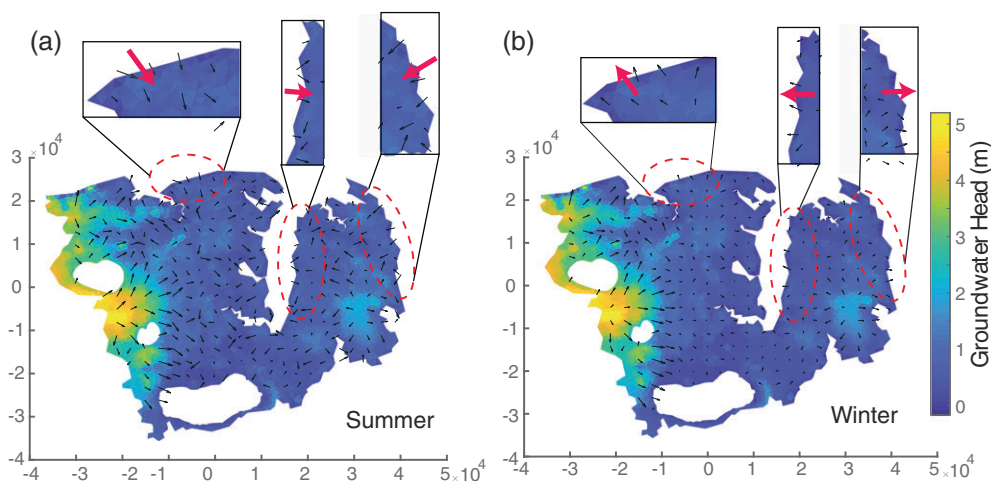


FIGURE 5 Climatological mean groundwater flow vectors across the study area in (a) winter and (b) summer seasons during 2007–2016. Arrows indicate the groundwater flow directions. The size of the arrows represents the speed of groundwater flow. The averaged flow speeds are 4.31 and 2.96 m³/day for summer and winter seasons, respectively. The colour bar indicates different mean groundwater head (m) in the winter and summer seasons from 2007 to 2016. High and low groundwater head is coded in a light and dark colour, separately. The red dashed circles highlight the areas where the directions of groundwater flow change in cold and warm seasons. The red arrows in the insets indicate the main flow directions in cold and warm seasons. The red arrows are not the actual groundwater flow vectors. The vertical and horizontal axes are the x and y geographic coordinates of the study domain (m)

4.2 | Impact area of coastal processes on GWT

Besides the topographic and climate controls on GWT, coastal processes, including SLR, tide, and saltwater intrusion, also affect groundwater dynamics. Here, the role of each coastal process in controlling GWT variation was examined by comparing the simulations with (a) only SLR (Exp. 1), (b) SLR and tide (Exp. 2), and (c) SLR, tide, and saltwater intrusion (Exp. 3).

The simulated GWT with only mean sea level (Exp. 1) is up to 0.6 m lower than the simulated GWT with both mean sea level and tide (Exp. 2, Figure 6a). Most of the inland and upland regions (dark red colour in Figure 6a) do not have significant difference in GWT (<0.001 m), while a large difference (>0.1 m) is found near the coastal boundary and the bank region of the Alligator River (light blue in Figure 6a), about 300–800 m from the coastline to the inland. Comparisons between Exp. 2 and Exp. 3 show that the simulated GWT without saltwater intrusion is slightly higher (<0.02 m) than that with saltwater intrusion for the majority of the study domain (green and light-yellow colours and negative value in Figure 6b), whereas the simulated GWT with saltwater intrusion is slightly higher than that without saltwater intrusion near the coastline (dark blue colour and negative value in Figure 6b). The GWT difference caused by saltwater intrusion process is about one order of magnitude smaller than that due to tide in the current climate with approximately 0.04-m rise of

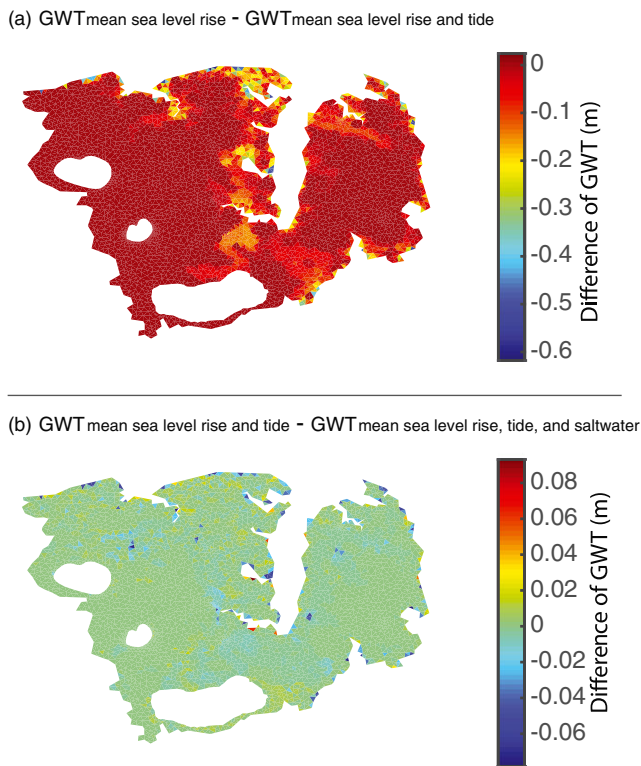


FIGURE 6 Spatial distribution of the difference of annual GWT (m) under different coastal processes. (a) The difference of annual GWT between simulations with only sea level rise and with sea level rise and tide. (b) The difference of annual GWT between the simulation with sea level rise and tide and the simulation with sea level rise, tide, and saltwater intrusion. Positive (negative) values on the colour bar mean that the simulated GWT from the former simulation is higher (lower) than that from latter simulation. GWT: groundwater table

sea level in the 10 years, revealing that tide should be the dominant coastal process controlling the variation of GWT.

4.3 | The influence of inundation on energy budget and ET

Besides the improvement of the representation of regional-scale hydrological interaction in PIHM-Wetland model, this study also improved the capability of the model in tracking the changes of energy budget and ET during inundation events because coastal wetlands are often partially or completely inundated (Nicholls, 2004). Results show that nearly half of the study area was inundated sometime during the 10-year period with an inundation frequency ranging from 5% (rarely inundated) to 100% (always inundated) each year (Figure 7). Two thirds of the time had a frequency higher than 50%. The occurrence of high-frequency inundation translates to a high frequency of change in land cover properties, which affects the energy budget and ET partitioning in the region.

In this subsection, simulated absorption of SW radiation during inundation was evaluated by considering the inundation effect and without considering the inundation effect. Then the impacts of inundation on total ET and ET partitioning were assessed by comparing the simulations with and without considering the inundation effect.

4.3.1 | Influence of inundation on the absorption of SW radiation

When no inundation occurs, net SW radiation is the same between the two simulations with and without considering the inundation effect. Thus, simulated net SW radiation from the two simulations are well aligned along the 1:1 line (the lower black dashed lines in Figure 8). However, when inundation occurs, the simulation considering the inundation effect predicts a higher net SW radiation because ponding water absorbs more and reflects less SW radiation than does the original land cover without inundation, represented by a linear regression line (the upper black dashed lines in Figure 8) with a higher slope. Specifically, the simulation considering the inundation effect predicts about 6% and 10% more SW radiation annually absorbed by the forested wetland and the herbaceous wetland, respectively. The

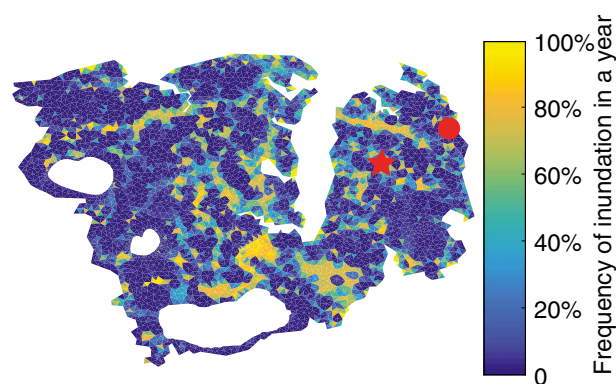


FIGURE 7 Distribution of inundation frequency in the 10-year simulation. The red star and dot denote model elements at the inland region and near the shoreline, representing the forested wetland and the coastal herbaceous wetland with the vegetation height around 20 m 0.25 m, respectively

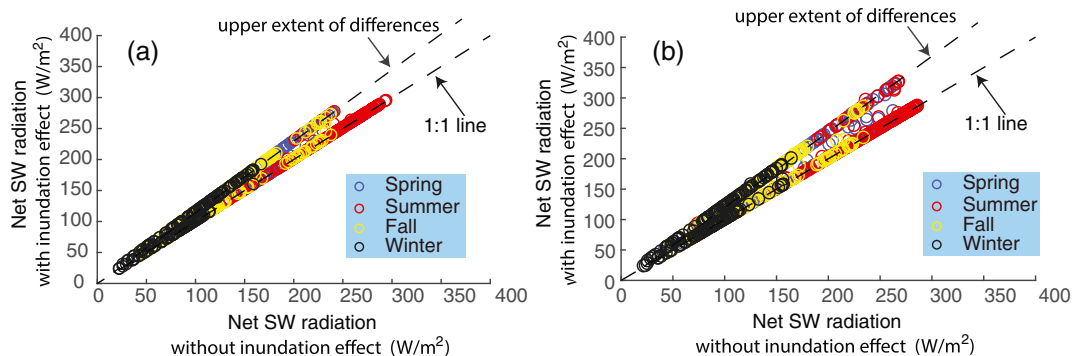


FIGURE 8 Comparison of simulated daily net SW radiation (W/m^2) with and without the inundation effect at (a) forested wetland (red star in Figure 7) and (b) coastal herbaceous wetland (red dot in Figure 7). The circles in blue, red, yellow, and black represent the net SW radiation in different seasons. The dashed lines are the regression lines that fit the data circles. The lower black dashed line (1:1 line) indicates no difference between the simulations. SW: shortwave

higher percentage of the increase of SW radiation at the herbaceous wetland is attributed to more frequent inundation due to coastal processes. Seasonally, for the forested wetlands, the inundation effect (red circles in Figure 8a) on net SW radiation is less apparent in summer (82% of red circles are along the lower line and 18% are on the upper line) than in the other seasons, because surface albedo does not change much due to fewer inundation events in summer. In contrast, for the coastal herbaceous wetland, a substantial number of red circles (47%) are on the upper line, indicating that the inundation effect on net SW radiation during the summer is apparent, and the seasonal differences of the inundation impact are smaller at the coastal herbaceous wetland mainly due to regulation by coastal processes. After a significance test, the difference between model simulations due to inundation is significant at the 1% level.

4.3.2 | Influence of inundation on total ET and ET partitioning

This study investigated the difference of simulated ET between the simulations with and without considering the inundation effect (orange and blue bars, Figure 9). Total ET in the simulations with inundation effect is about 13%, 2%, 8%, and 10% higher than the

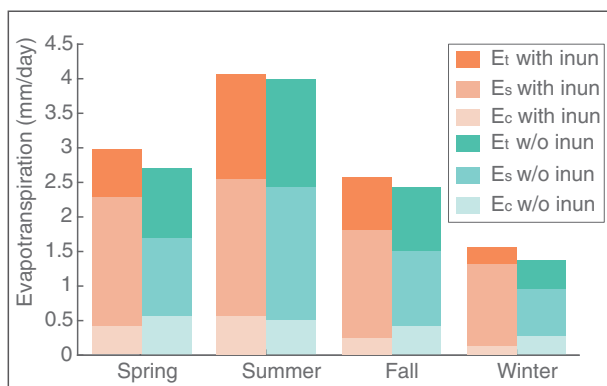


FIGURE 9 Seasonal variation of total ET and ET partitioning of the simulation considering inundation effect (abbreviated as “with inun” for the orange bars) and not considering inundation effect (abbreviated as “w/o inun” for the blue bars). E_c , E_s , and E_t are canopy evaporation (mm/day), soil evaporation (mm/day), and transpiration (mm/day), respectively. ET: evapotranspiration

simulated ET without considering the inundation effect in the spring, summer, fall, and winter, respectively, mainly due to the difference in absorbed radiation during inundation between the simulations. The smaller differences of summer ET between the two simulations are mainly because of the lower frequency of inundation in summer (Figure 9) compared with the other seasons.

Inundation can also affect ET partitioning by changing canopy evaporation and transpiration when surface water is higher than the height of the vegetation canopy. We modelled the variation of hourly soil evaporation (E_s), transpiration (E_t), and canopy evaporation (E_c) at the coastal herbaceous wetland (black star in Figure 7) during a 6-day window (from 12:00 p.m. on Sept 26, 2007, to 12:00 p.m. on Oct 2, 2007; Figure 10). The 6-day window was selected because it includes different intensities of rainfall rate and inundation and, thus, is a representative period for understanding the influence of inundation caused by coastal processes and climate events on ET partitioning. The 6-day window was divided into five segments to illustrate the different roles of rainfall and inundation on ET (Figure 10). Segment 1 is from time $t = 0$ to $t = t_1$ with large rainfall but low inundation level (lower than the canopy height; green dashed line in Figure 10c). At the beginning of Segment 1, the E_t rate is two times smaller than E_c . Then the E_t drops to zero when the canopy is totally wet during large rainfall events because the driver of transpiration, VPG, between the plant stomata and atmosphere, becomes zero. Thus, in Segment 1, the relative importance of inundation on E_c and E_t is minor; rainfall plays a more important role on E_c and E_t . Subsequently, in Segment 2 (from $t = t_1$ to $t = t_2$), the E_c decreases to zero as well because surface water completely submerges the vegetation canopy (inundation level > canopy height). During Segment 3 (from $t = t_2$ to $t = t_3$), the E_c quickly increases when the inundation level declines but drops to zero again when the inundation level is again higher than the canopy height. During Segment 4 ($t = t_3$ to $t = t_5$), the rainfall stops, but E_t and E_c are still equal to zero during the daytime because the SWL is higher than the vegetation canopy during daytime. A large increase of E_t is observed before $t = t_4$ when the SWL is lower than the vegetation canopy during daytime. However, E_t declines to zero quickly when the canopy is again submerged in surface water after $t = t_4$. The change of ET during Segments 2, 3, and 4 demonstrate the dominant control of inundation

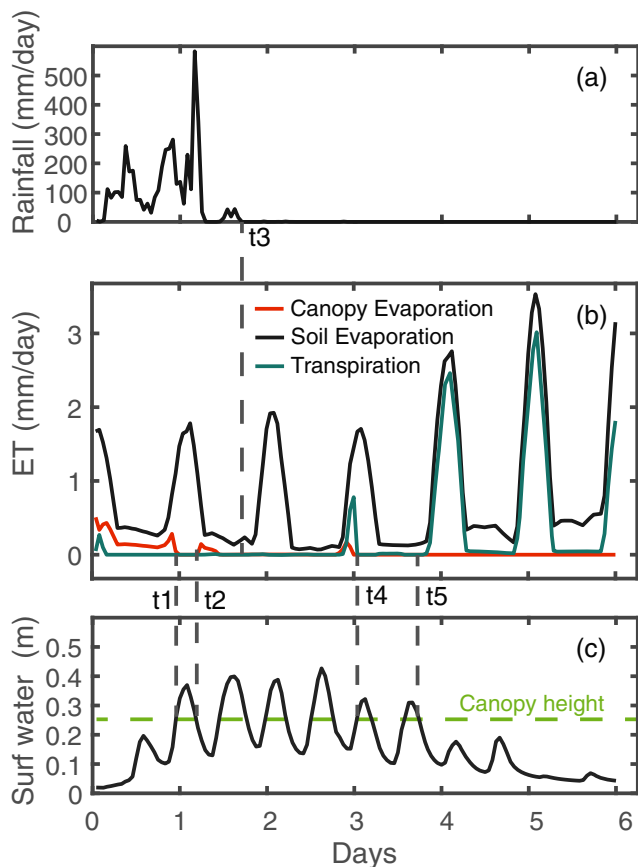


FIGURE 10 Change of ET partitioning (mm/day) under the variations of rainfall (mm/day) and surface water depth (m) of the model element near the coast (red dot in Figure 7). Time series of (a) rainfall, (b) ET partitioning (canopy evaporation E_c , soil evaporation E_s , and transpiration E_t), and (c) surface water depth (m). x-axis: Day = 0 refers to 12:00 p.m. of September 26, 2007 (local time). ET: evapotranspiration

on E_c and E_t . During Segment 5 (after $t = t_5$), E_t significantly increases when the SWL is lower than the canopy height, and the influence of inundation on E_c and E_t decreases.

In summary, when inundation level is higher than the vegetation canopy, E_c and E_t do not contribute to total ET because both decrease to zero. This is illustrated where the 10-year averaged seasonal E_c and E_t at the herbaceous wetland (black star in Figure 7) from the simulation considers the inundation effect (orange bars in Figure 9) are smaller than E_c and E_t from the simulation without inundation (blue bars in Figure 9). The differences of E_c and E_t are more obvious in the spring, fall, and winter seasons when both the magnitude and frequency of inundation events are higher than those in the summer season.

5 | DISCUSSION

5.1 | Understanding of coastal wetland hydrology

5.1.1 | Topography-controlled or recharge-controlled GWT in the coastal wetlands?

Previous studies classified the GWT at the east coast of the United States as a topography-controlled GWT system based on a global

coastal region classification approach that defines a ratio between potential GWT rise and topographic rise (Gleeson, Marklund, Smith, & Manning, 2011; Michael, Russoniello, & Byron, 2013). Our simulation (e.g., Figure 5) confirmed that the GWT in the upland is primarily topography-controlled GWT. Thus, water supply from the upland is important for retaining the GWT of the lowland region. Additionally, our analysis found that the topographic control is weakened with the decrease in elevation gradient, where the amount of precipitation becomes the dominant factor controlling groundwater recharge and GWT variation at the land–ocean interface (recharge-controlled GWT). Less recharge (e.g., in the summer season) would result in the decline of fresh GWT at the land–ocean interface and thus stimulate saltwater intrusion. Conversely, high recharge (e.g., in the winter season) would raise GWT and thus significantly prevent the intrusion of salt water.

5.1.2 | Influence of coastal processes on coastal land use planning

This study found that coastal processes can increase the water level by up to 0.6 m over the coastal wetland and can influence a distance spanning 300–800 m from the coastline to the inland. This 300- to 800-m zone is an area where freshwater and saltwater processes are in balance at *annual* scales. However, such an area will vary significantly under short-term coastal events, such as diurnal, daily, weekly, and seasonal scale events, which remain to be investigated.

In the 10-year simulation period, tides are found to be the dominant control on GWT variation. The influences of mean sea level and saltwater intrusion on GWT are an order of magnitude smaller than those of local tides. In the future, when climate becomes much warmer (Nicholls & Cazenave, 2010) and SLRs much higher, this conclusion may have to be revisited.

The analysis of the impact area of coastal processes is important for land use planning under projected coastal SLR. The estimated impact areas of coastal processes are particularly vulnerable to future SLR. City planners should avoid such areas for urban development and farming. In addition, the distributed model developed here can effectively support infrastructure design and modelling in the coastal wetland regions.

5.1.3 | Influence of inundation on regional water, energy, and geochemical cycles

To the best of our knowledge, this is the *first* modelling study that takes into account the effect of inundation in hydrological and energy cycles at regional scales. The amount of increase in water loss due to wetland inundation may significantly change the hydrological cycle by decreasing effective rainfall and SWC and increasing depth to the GWT. Variations in ET and ET partitioning also affect the feedbacks between land and the lower boundary of atmosphere, which is one of the key processes in earth system modelling. Thus, the inundation process should be included in a realistic regional/global climate model to capture the unique atmosphere–land feedback of coastal wetlands.

Simulated inundation effects show that inundation may significantly decrease canopy evaporation and plant transpiration, especially for the herbaceous wetlands. Frequent inundation events submerge vegetation and, as a result, decrease the contributions of transpiration

and canopy evaporation to total ET. The decrease in transpiration corresponds to a decrease in plant water uptake from the soil and subsequently affects sediment oxidation (Dacey & Howes, 1984) and nutrient uptake (Alam, 1999; Jackson & Colmer, 2005), such as for nitrate, thereby potentially influencing the geochemical cycle and plant nutrition of coastal wetland ecosystems.

5.2 | PIHM-Wetland as a tool for wetland hydrological modelling

Like all models, PIHM-Wetland involves trade-offs between simplicity and realism, speed and resolution. The model's design reflects the purpose of providing a physically based intermediate model linking the small-scale and large-scale models. PIHM-Wetland is unique because it has the capability to examine hydrological interactions over a wide range of landscape components that influence the characteristics of wetland hydrology (Figures 5 and 6) and track the detailed surface and subsurface hydrological change (Figures 7, 8, 9, and 10). Our model uses readily available national and international datasets that allow model parameterization at a regional scale while detailed hydrological processes are still retained.

5.3 | Limitations and future work

Model evaluation suggests that PIHM-Wetland reasonably captures the complex hydrological behaviours of coastal wetlands in eastern North Carolina (Section 3.3). However, this assessment could be affected by several factors. First, the model input data, NLDAS-2, is a reanalysis product that contains uncertainties from the original observations and data assimilation techniques (Xia et al., 2012). Comparison between NLDAS-2 and the observed meteorological variables (Section 3.2.2) indicates that the NLDAS-2 product agrees well with the in situ measurements at the ARCW, except for precipitation at the daily timescale. This discrepancy, to some extent, may lead to simulation uncertainty. However, it is worth noticing that the scatter plot may not represent the actual precipitation because of the scale mismatch between the NLDAS grid (0.125 degree) and the point-scale observations. Additionally, this study used the tide and sea level observation from the closest national site (15 km away from the model boundary) near the study area, ignoring the possible time delay of the tide processes when it actually reaches the coastal boundary. Second, the limited number of sites with validation data implies uncertainties for extrapolation to regional scales. However, the model was evaluated by the best available observations, and our two observation sites (one forested wetland and one herbaceous marsh) represent the two major ecosystem types in the study region (75% are forested wetlands and 3% are marshes). The distributions of topography, soil properties (Table S1), and land cover (Table S2) are relatively homogeneous. The agreement between the model simulation and observations at the two sites confirmed that the model reasonably captures the dynamics of the GWT, ET, and SWC. Continued evaluation of the model at the regional scale is needed when more observational data are available. Our model simulations, such as for the distribution of inundation frequency (Figure 7), provide important guidance for the design of future observation sites.

Wetland ecophysiological processes should be explicitly considered in further model development. Future sea level is expected to rise by ~30 to 180 cm (Nicholls & Cazenave, 2010), which will significantly affect ET and energy budgets of coastal wetlands. SLR can also be expected to affect plant physiology; for example, flood-intolerant vegetation will become stressed or will die (Conner, Mihalia, & Wolfe, 2002). Water salinity can also impact the physiology of many freshwater-dependent wetland plants (e.g., Krauss et al. (2009)).

This study provides a foundation towards coupling wetland hydrology and biogeochemical processes. Wetlands represent a large carbon pool, serving as terrestrial carbon sinks, and also as a source of CH₄ emissions. Water table depth is a key control on the dynamics of CO₂ and CH₄ fluxes (Fan & Miguez-Macho, 2011; Lafleur, 2008). A drop in the GWT may stimulate soil respiration, and greater CO₂ release from wetland soils (Miao et al., 2013; Mitsch et al., 2013), whereas a decrease in GWT may cause a wetland switch from a CH₄ source to a sink (Whalen, 2005).

6 | CONCLUSIONS

This study presented a new regional-scale, process-based hydrological model, PIHM-Wetland, which couples coastal processes (tide, SLR, and saltwater intrusion) with surface and subsurface hydrological processes and considers the influence of inundation on wetland hydrology. We show that PIHM-Wetland is accurate at simulating observations and the essential features of hydrological processes of representative coastal wetlands in eastern North Carolina, USA.

PIHM-Wetland offers a practical tool for quantifying wetland hydrology. First, it has the capacity to describe the spatial variation of groundwater flow and SWL (e.g., inundation) across the regional wetland domain. Second, PIHM-Wetland simulation showed that coastal processes result in a higher daily GWT throughout the wetland domain compared with simulations without coastal processes. The influence of coastal processes can extend 300–800 m from the shoreline. Third, PIHM-Wetland is capable of tracking the impact of inundation on energy budgets and the hydrological cycle. Inundation also influences the contributions of transpiration and canopy evaporation to total ET when the inundation level is higher than canopy height, especially in cool seasons.

PIHM-Wetland represents more than just a coastal wetland model, as it can also be applied to inland wetlands. The hydrological processes described in the model can be representative of the hydrological processes in inland wetlands, and the coastal boundary conditions can be easily turned off to fit hydrological characteristics of inland wetlands.

ACKNOWLEDGMENTS

We thank Dr. Christopher Duffy for the suggestions on the coastal processes coupling. Support for this project was provided by the multiagency Carbon Cycle Science Program (A.5) through USDA National Institute of Food and Agriculture Award 2014-67003-22068 and an Ameriflux Core Site Network Management award (Lawrence Berkeley National Laboratory 2014-0500/7090112). We would like to acknowledge the high-performance computing support

from Yellowstone and Cheyenne provided by NCAR's Computational and Information Systems Laboratory, sponsored by the National Science Foundation. Surface water data acquisition was supported by NSF Awards Division of Emerging Frontiers EF-1427188 and Division of Earth Sciences EAR-1462169 with the help of Theo Jass. The model, input data, and simulated results are available upon request at this moment and will be available at the official github repository (<https://github.com/wetland-hydro/PIHM-Wetland.git>) soon.

ORCID

Yu Zhang  <http://orcid.org/0000-0002-9263-8428>

REFERENCES

- Alam, S. M. (1999). Nutrient uptake by plants under stress conditions. *Handbook of Plant and Crop Stress*, 2, 285–313.
- Ataie-Ashtiani, B., Volker, R., & Lockington, D. (1999). Tidal effects on sea water intrusion in unconfined aquifers. *Journal of Hydrology*, 216(1), 17–31.
- Bao, C., Li, L., Shi, Y., & Duffy, C. (2017). Understanding watershed hydrogeochemistry: 1. Development of RT-Flux-PIHM. *Water Resources Research*, 53, 2328–2345.
- Braun, J., & Sambridge, M. (1997). Modelling landscape evolution on geological time scales: A new method based on irregular spatial discretization. *Basin Research*, 9(1), 27–52.
- Bruland, G. L., & Richardson, C. J. (2006). Comparison of soil organic matter in created, restored and paired natural wetlands in North Carolina. *Wetlands Ecology and Management*, 14(3), 245–251. <https://doi.org/10.1007/s11273-005-1116-z>
- Byrne, G. D. (1992). Pragmatic experiments with Krylov methods in the stiff ODE setting. Paper presented at the Institute of Mathematics and Its Applications Conference Series.
- Cahoon, D. R., Hensel, P. F., Spencer, T., Reed, D. J., McKee, K. L., & Saintilan, N. (2006). Coastal wetland vulnerability to relative sea-level rise: Wetland elevation trends and process controls. *Wetlands and Natural Resource Management*, 271–292.
- Chen, F., Mitchell, K., Schaake, J., Xue, Y., Pan, H. L., Koren, V., ... Betts, A. (1996). Modeling of land surface evaporation by four schemes and comparison with FIFE observations. *Journal of Geophysical Research-Atmospheres*, 101(D3), 7251–7268.
- Cohen, S. D., & Hindmarsh, A. C. (1996). CVODE, a stiff/nonstiff ODE solver in C. *Computers in Physics*, 10(2), 138–143.
- Conner, W. H., Mihalja, I., & Wolfe, J. (2002). Tree community structure and changes from 1987 to 1999 in three Louisiana and three South Carolina forested wetlands. *Wetlands*, 22(1), 58–70.
- Dacey, J. W., & Howes, B. L. (1984). Water uptake by roots controls water table movement and sediment oxidation in short *Spartina* marsh. *Science*, 224, 487–490.
- Dai, Z., Trettin, C. C., Li, C., Amatya, D. M., Sun, G., & Li, H. (2010). Sensitivity of stream flow and water table depth to potential climatic variability in a coastal forested watershed. *JAWRA Journal of the American Water Resources Association*, 46(5), 1036–1048.
- Day, J. W., Christian, R. R., Boesch, D. M., Yáñez-Arancibia, A., Morris, J., Twilley, R. R., ... Schaffner, L. (2008). Consequences of climate change on the ecogeomorphology of coastal wetlands. *Estuaries and Coasts*, 31(3), 477–491.
- Dickinson, E., Henderson-Sellers, A., & Kennedy, J. (1993). Biosphere-atmosphere transfer scheme (BATS) version 1e as coupled to the NCAR community climate model.
- Erwin, K. L. (2009). Wetlands and global climate change: the role of wetland restoration in a changing world. *Wetlands Ecology and Management*, 17(1), 71.
- Fan, Y., & Miguez-Macho, G. (2011). A simple hydrologic framework for simulating wetlands in climate and earth system models. *Climate Dynamics*, 37(1–2), 253–278.
- Fry, J. A., Xian, G., Jin, S., Dewitz, J. A., Homer, C. G., Limin, Y., ... Wickham, J. D. (2011). Completion of the 2006 National Land Cover Database for the conterminous United States. *Photogrammetric Engineering and Remote Sensing*, 77(9), 858–864.
- Gleeson, T., Marklund, L., Smith, L., & Manning, A. H. (2011). Classifying the water table at regional to continental scales. *Geophysical Research Letters*, 38(5).
- Gupta, A. D. (1985). Approximation of salt-water interface fluctuation in an unconfined coastal aquifer. *Ground Water*, 23(6), 783–794. <https://doi.org/10.1111/j.1745-6584.1985.tb01958.x>
- Hinrichsen, D. (1999). *Coastal waters of the world: Trends, threats, and strategies*. USA: Island Press.
- Jackson, M., & Colmer, T. (2005). Response and adaptation by plants to flooding stress. *Annals of Botany*, 96(4), 501–505.
- Kirwan, M. L., & Magonigal, J. P. (2013). Tidal wetland stability in the face of human impacts and sea-level rise. *Nature*, 504(7478), 53.
- Kolb, K. H. (1974). Critical problems of the coastal zone. *SAIS Review*, 18(3), 24.
- Koster, R. D., & Suarez, M. J. (1992). Modeling the land surface boundary in climate models as a composite of independent vegetation stands. *Journal of Geophysical Research-Atmospheres*, 97(D3), 2697–2715.
- Krauss, K. W., Duberstein, J. A., Doyle, T. W., Conner, W. H., Day, R. H., Inabinet, L. W., & Whitbeck, J. L. (2009). Site condition, structure, and growth of baldcypress along tidal/non-tidal salinity gradients. *Wetlands*, 29(2), 505–519.
- Kumar, M. (2009). *Toward a hydrologic modeling system*. (Ph.D.), Pennsylvania State University, Retrieved from: <http://etda.libraries.psu.edu/theses/approved/WorldWideIndex/ETD-4264/index.html>
- Kumar, M., Bhatt, G., & Duffy, C. J. (2009). An efficient domain decomposition framework for accurate representation of geodata in distributed hydrologic models. *International Journal of Geographical Information Science*, 23(12), 1569–1596. <https://doi.org/10.1080/13658810802344143>
- La Torre Torres, I. B., Amatya, D. M., Sun, G., & Callahan, T. J. (2011). Seasonal rainfall-runoff relationships in a lowland forested watershed in the southeastern USA. *Hydrological Processes*, 25(13), 2032–2045.
- Lafleur, P. M. (2008). Connecting atmosphere and wetland: Energy and water vapour exchange. *Geography Compass*, 2(4), 1027–1057.
- Land Data Assimilation System. (1999). Mapped monthly vegetation data from Goddard Space Flight Center, NASA. Retrieved from: <https://ldas.gsfc.nasa.gov/nldas/web/web.veg.monthly.table.html>
- Leonard, L., & Duffy, C. J. (2013). Essential terrestrial variable data workflows for distributed water resources modeling. *Environmental Modelling & Software*, 50, 85–96.
- Li, L., Bao, C., Sullivan, P. L., Brantley, S., Shi, Y., & Duffy, C. (2017). Understanding watershed hydrogeochemistry: 2. Synchronized hydrological and geochemical processes drive stream chemostatic behavior. *Water Resources Research*, 53(3), 2346–2367.
- Li, L., Barry, D., & Pattiaratchi, C. (1997). Numerical modelling of tide-induced beach water table fluctuations. *Coastal Engineering*, 30(1–2), 105–123.
- Li, L., Barry, D., Stagnitti, F., & Parlange, J. Y. (1999). Submarine groundwater discharge and associated chemical input to a coastal sea. *Water Resources Research*, 35(11), 3253–3259.
- Li, S., & Duffy, C. J. (2011). Fully coupled approach to modeling shallow water flow, sediment transport, and bed evolution in rivers. *Water Resources Research*, 47(3), n/a–n/a. <https://doi.org/10.1029/2010wr009751>
- Li, W., Li, L., Fu, R., Deng, Y., & Wang, H. (2011). Changes to the North Atlantic subtropical high and its role in the intensification of summer rainfall variability in the southeastern United States. *Journal of Climate*, 24(5), 1499–1506.

- Li, Z., & Garand, L. (1994). Estimation of surface albedo from space: A parameterization for global application. *Journal of Geophysical Research-Atmospheres*, 99(D4), 8335–8350.
- Li, Z.-L., Wu, H., Wang, N., Qiu, S., Sobrino, J. A., Wan, Z., ... Yan, G. (2013). Land surface emissivity retrieval from satellite data. *International Journal of Remote Sensing*, 34(9–10), 3084–3127.
- Liu, Y., & Kumar, M. (2016). Role of meteorological controls on interannual variations in wet-period characteristics of wetlands. *Water Resources Research*, 52(7), 5056–5074.
- Lu, J., Sun, G., McNulty, S. G., & Amatya, D. M. (2003). Modeling actual evapotranspiration from forested watersheds across the Southeastern United States. *JAWRA Journal of the American Water Resources Association*, 39(4), 886–896.
- Merken, R., Deboelpaep, E., Teunen, J., Saura, S., & Koedam, N. (2015). Wetland suitability and connectivity for trans-Saharan migratory waterbirds. *PLoS One*, 10(8), e0135445.
- Miao, G., Noormets, A., Domec, J. C., Trettin, C. C., McNulty, S. G., Sun, G., & King, J. S. (2013). The effect of water table fluctuation on soil respiration in a lower coastal plain forested wetland in the southeastern US. *Journal of Geophysical Research - Biogeosciences*, 118(4), 1748–1762.
- Michael, H. A., Mulligan, A. E., & Harvey, C. F. (2005). Seasonal oscillations in water exchange between aquifers and the coastal ocean. *Nature*, 436(7054), 1145–1148.
- Michael, H. A., Russoniello, C. J., & Byron, L. A. (2013). Global assessment of vulnerability to sea-level rise in topography-limited and recharge-limited coastal groundwater systems. *Water Resources Research*, 49(4), 2228–2240.
- Mitsch, W. J., Bernal, B., Nahlik, A. M., Mander, Ü., Zhang, L., Anderson, C. J., ... Brix, H. (2013). Wetlands, carbon, and climate change. *Landscape Ecology*, 28(4), 583–597.
- Moorhead, K. K., & Brinson, M. M. (1995). Response of wetlands to rising sea level in the lower coastal plain of North Carolina. *Ecological Applications*, 5(1), 261–271.
- Moriasi, D. N., Arnold, J. G., Van Liew, M. W., Bingner, R. L., Harmel, R. D., & Veith, T. L. (2007). Model evaluation guidelines for systematic quantification of accuracy in watershed simulations. *Transactions of the ASABE*, 50(3), 885–900.
- Morris, J. T., Sundareshwar, P., Nietch, C. T., Kjerfve, B., & Cahoon, D. R. (2002). Responses of coastal wetlands to rising sea level. *Ecology*, 83(10), 2869–2877.
- Mu, Q., Zhao, M., & Running, S. W. (2011). Improvements to a MODIS global terrestrial evapotranspiration algorithm. *Remote Sensing of Environment*, 115(8), 1781–1800.
- Nash, J. E., & Sutcliffe, J. V. (1970). River flow forecasting through conceptual models part I—A discussion of principles. *Journal of Hydrology*, 10(3), 282–290.
- National Research Council (1995). *Wetlands: Characteristics and boundaries*. National Academies Press.
- Nicholls, R. J. (2004). Coastal flooding and wetland loss in the 21st century: changes under the SRES climate and socio-economic scenarios. *Global Environmental Change*, 14(1), 69–86.
- Nicholls, R. J., & Cazenave, A. (2010). Sea-level rise and its impact on coastal zones. *Science*, 328(5985), 1517–1520.
- Niu, G. Y., Yang, Z. L., Mitchell, K. E., Chen, F., Ek, M. B., Barlage, M., ... Rosero, E. (2011). The community Noah land surface model with multiparameterization options (Noah-MP): 1. Model description and evaluation with local-scale measurements. *Journal of Geophysical Research-Atmospheres*, 116(D12).
- NOAA Habitat Conservation. (2017). Coastal wetlands: too valuable to lose. Retrieved from: <https://www.fisheries.noaa.gov/coastal-wetlands-too-valuable-lose>
- O'Neill, R., Hunsaker, C., Timmins, S. P., Jackson, B., Jones, K., Riitters, K. H., & Wickham, J. D. (1996). Scale problems in reporting landscape pattern at the regional scale. *Landscape Ecology*, 11(3), 169–180.
- Oude Essink, G., Van Baaren, E. S., & De Louw, P. G. (2010). Effects of climate change on coastal groundwater systems: A modeling study in the Netherlands. *Water Resources Research*, 46(10).
- Pendleton, L., Donato, D. C., Murray, B. C., Crooks, S., Jenkins, W. A., Siffleet, S., ... Marbà, N. (2012). Estimating global “blue carbon” emissions from conversion and degradation of vegetated coastal ecosystems. *PLoS One*, 7(9), e43542.
- Qu, Y., & Duffy, C. J. (2007). A semidiscrete finite volume formulation for multiprocess watershed simulation. *Water Resources Research*, 43(8), 1–18. <https://doi.org/10.1029/2006wr005752>
- Rawson, H., Begg, J., & Woodward, R. (1977). The effect of atmospheric humidity on photosynthesis, transpiration and water use efficiency of leaves of several plant species. *Planta*, 134(1), 5–10.
- Rebelo, L.-M., Senay, G., & McCartney, M. P. (2012). Flood pulsing in the Sudd wetland: Analysis of seasonal variations in inundation and evaporation in South Sudan. *Earth Interactions*, 16(1), 1–19.
- Robinson, C., Gibbes, B., & Li, L. (2006). Driving mechanisms for groundwater flow and salt transport in a subterranean estuary. *Geophysical Research Letters*, 33(3).
- Rollins, M. G. (2009). LANDFIRE: A nationally consistent vegetation, wildland fire, and fuel assessment. *International Journal of Wildland Fire*, 18(3), 235–249.
- Roulet, N. (1990). The hydrological role of peat-covered wetlands. *The Canadian Geographer/Le Géographe Canadien*, 34(1), 82–83.
- Sánchez-Carrillo, S., Angeler, D. G., Sánchez-Andrés, R., Alvarez-Cobelas, M., & Garatza-Payán, J. (2004). Evapotranspiration in semi-arid wetlands: Relationships between inundation and the macrophyte-cover: open-water ratio. *Advances in Water Resources*, 27(6), 643–655.
- Schwerdtfeger, J., da Silveira, S. W. G., Zeilhofer, P., & Weiler, M. (2015). Coupled ground-and space-based assessment of regional inundation dynamics to assess impact of local and upstream changes on evaporation in tropical wetlands. *Remote Sensing*, 7(8), 9769–9795.
- Sellers, P., Mintz, Y., Sud, Y. E. A., & Dalcher, A. (1986). A simple biosphere model (SiB) for use within general circulation models. *Journal of the Atmospheric Sciences*, 43(6), 505–531.
- Shamir, U., & Dagan, G. (1971). Motion of the seawater interface in coastal aquifers: A numerical solution. *Water Resources Research*, 7(3), 644–657.
- Shi, Y., Baldwin, D. C., Davis, K. J., Yu, X., Duffy, C. J., & Lin, H. (2015). Simulating high resolution soil moisture patterns in the shale hills watershed using a land surface hydrologic model. *Hydrological Processes*.
- Shi, Y., Davis, K. J., Duffy, C. J., & Yu, X. (2013). Development of a coupled land surface hydrologic model and evaluation at a critical zone observatory. *Journal of Hydrometeorology*, 14(5).
- Smith, L., & Chapman, D. S. (1983). On the thermal effects of groundwater flow: 1. Regional scale systems. *Journal of Geophysical Research*, 88(B1), 593–608. <https://doi.org/10.1029/JB088iB01p00593>
- Staff, S. S. (2016). The Gridded Soil Survey Geographic (SSURGO) database for North Carolina from United States Department of Agriculture, Natural Resources Conservation Service. Retrieved from: <http://datagateway.nrcs.usda.gov/>
- Sumner, D. M., Wu, Q., & Pathak, C. S. (2011). Variability of albedo and utility of the MODIS albedo product in forested wetlands. *Wetlands*, 31(2), 229–237.
- Sun, G., Riekerk, H., & Comerford, N. B. (1998). Modeling the hydrologic impacts of forest harvesting on Florida flatwoods. *JAWRA Journal of the American Water Resources Association*, 34(4), 843–854.
- Taiz, L., Zeiger, E., Møller, I. M., & Murphy, A. (2015). *Plant physiology and development*. USA: Sinauer Associates, Incorporated.
- Tiner, R. W. (1999). *Wetland indicators: A guide to wetland identification, delineation, classification, and mapping*. USA: CRC press.
- Tiner, R. W. (2013). *Tidal wetlands primer*. USA: University of Massachusetts Press.

- Van Genuchten, M. T. (1980). A closed-form equation for predicting the hydraulic conductivity of unsaturated soils. *Soil Science Society of America Journal*, 44(5), 892–898.
- Vergnes, J.-P., Decharme, B., Alkama, R., Martin, E., Habets, F., & Douville, H. (2012). A simple groundwater scheme for hydrological and climate applications: Description and offline evaluation over France. *Journal of Hydrometeorology*, 13(4), 1149–1171.
- Whalen, S. (2005). Biogeochemistry of methane exchange between natural wetlands and the atmosphere. *Environmental Engineering Science*, 22(1), 73–94.
- Woo, M.-K. (1992). Impacts of climate variability and change on Canadian wetlands. *Canadian Water Resources Journal*, 17(1), 63–69.
- Wösten, J., Pachepsky, Y. A., & Rawls, W. (2001). Pedotransfer functions: Bridging the gap between available basic soil data and missing soil hydraulic characteristics. *Journal of Hydrology*, 251(3), 123–150.
- Xia, Y., Mitchell, K., Ek, M., Sheffield, J., Cosgrove, B., Wood, E., ... Meng, J. (2012). Continental-scale water and energy flux analysis and validation for the North American Land Data Assimilation System project phase 2 (NLDAS-2): 1. Intercomparison and application of model products. *Journal of Geophysical Research-Atmospheres*, 117(D3), 1–27.
- Yu, X., Bhatt, G., Duffy, C. J., Wardrop, D. H., Najjar, R. G., Ross, A. C., & Rydzik, M. (2015). A coupled surface subsurface modeling framework to assess the impact of climate change on freshwater wetlands. *Climate Research*, 66(3), 211–228.
- Yu, X., Duffy, C., Baldwin, D. C., & Lin, H. (2014). The role of macropores and multi-resolution soil survey datasets for distributed surface–subsurface flow modeling. *Journal of Hydrology*.
- Yu, X., Duffy, C., Kaye, J., Crow, W., Bhatt, G., & Shi, Y. (2014). Watershed reanalysis of water and carbon cycle models at a critical zone observatory. *Remote Sensing of the Terrestrial Water Cycle*, 206, 493.
- Yu, X., Duffy, C., Zhang, Y., Bhatt, G., & Shi, Y. (2016). Virtual experiments guide calibration strategies for a real-world watershed application of coupled surface–subsurface modeling. *Journal of Hydrologic Engineering*, 21(11), 04016043.
- Yu, X., Yang, J., Graf, T., Koneshloo, M., O'Neal, M. A., & Michael, H. A. (2016). Impact of topography on groundwater salinization due to ocean surge inundation. *Water Resources Research*, 52(8), 5794–5812.
- Yuan, L. R., Xin, P., Kong, J., Li, L., & Lockington, D. (2011). A coupled model for simulating surface water and groundwater interactions in coastal wetlands. *Hydrological Processes*, 25(23), 3533–3546.
- Zhang, Y., Slingerland, R., & Duffy, C. (2016). Fully-coupled hydrologic processes for modeling landscape evolution. *Environmental Modelling & Software*, 82, 89–107.
- Zhang, Y., Yang, S., Ouyang, W., Zeng, H., & Cai, M. (2010). Applying multi-source remote sensing data on estimating ecological water requirement of grassland in ungauged region. *Procedia Environmental Sciences*, 2, 953–963.
- Zhu, J., Sun, G., Li, W., Zhang, Y., Miao, G., Noormets, A., ... Wang, X. (2017). Modeling the potential impacts of climate change on the hydrology of selected forested wetlands in the Southeastern United States. *Hydrology and Earth System Sciences*. <https://doi.org/10.5194/HESS-21-6289-2017>

SUPPORTING INFORMATION

Additional supporting information may be found online in the Supporting Information section at the end of the article.

How to cite this article: Zhang Y, Li W, Sun G, et al. Understanding coastal wetland hydrology with a new regional-scale, process-based hydrological model. *Hydrological Processes*. 2018;32:3158–3173. <https://doi.org/10.1002/hyp.13247>